SAKARYA ÜNİVERSİTESİ
FEN BİLİMLERİ ENSTİTÜSÜ DERGİSİ

Sakarya University Journal of Science
SAUJS

ISSN 1301-4048 e-ISSN 2147-835X Period Bimonthly Founded 1997 Publisher Sakarya University
http://www.saujs.sakarya.edu.tr/

Title: A New Novel Synchronization Index of Brain Networks in Hyperbolic EEG Dynamics

Authors: Rüştü Murat DEMİRER

Recieved: 2021-09-22 00:00:00

Accepted: 2022-05-06 00:00:00

Article Type: Research Article

Volume: 26
Issue: 3
Month: June
Year: 2022
Pages: 600-607

How to cite
Rüştü Murat DEMİRER; (2022), A New Novel Synchronization Index of Brain Networks in Hyperbolic EEG Dynamics. Sakarya University Journal of Science, 26(3), 600-607, DOI: 10.16984/saufenbilder.999015
Access link
http://www.saujs.sakarya.edu.tr/tr/pub/issue/70993/999015

Sakarya University Journal of Science 26(3), 600-607, 2022

A New Novel Synchronization Index of Brain Networks in Hyperbolic EEG Dynamics

Rüştü Murat DEMİRER*[1]

Abstract

The functional connectivity of brain connectivity changes its pattern over time i.e. dynamics, even in the resting state with an infinite number of degrees of freedom with local couplings. Recently, quantifying the level of synchrony has received considerable attention. We hypothesized that time-varying instantaneous phase synchronization over local couplings are defined in hyperbolic space and different brain regions can identify failures, flexibility, and stability in network dynamics. Our goal is to understand the phase synchronization changes of the beta-gamma band, and in addition, to investigate Shannon entropy based on phase synchronization stability. Whole EEG dynamics from local phase synchronizations was used to detect treatment resistance from both hemispheres in OCD patients. Temporal filtering and Hilbert transforms were performed to infer beta-gamma band phase difference activity from the EEG brain dynamics. Then, the response beta-gamma band phase stability was quantified using a new phase synchronization index (PSI). Results indicated significantly changed phase synchronization of the response and non-response to treatment, patients in OCD patients in F7 electrode. Greater phase fluctuations of beta-gamma synchronizations in treatment resistance OCD is claiming phase deficiencies within neural populations. This study first provides experimental and theoretical support for characterizing cycle structure depends on the non-Euclidian dynamics of neural phase synchrony caused by disturbances of underlying neurotransmitter systems, as reflected in different normal and disease states.

Keywords: Hilbert Transform Shannon Entropy, SVM algorithm, Tass Synchronization

1. INTRODUCTION

Structural and functional interactions do not only depend on the strength of the number of neuron activations but also depend on how often we pick the spikes but the precise timing of the spikes underlying neural assemblies is also essential to the brain dynamics with coherent and incoherent dynamics. The phase synchronizations may be a general neural pattern for representing sequential events for learning, plasticity, and memory [1].

* Corresponding author: murat.demirer@isikun.edu.tr
[1] Işik University, Faculty of Engineering and Natural Sciences, Department of Electrical-Electronic Engineering
ORCID: https://orcid.org/0000-0002-5508-741X

The idea of phase synchronization (PS) is to understand the precise timing among brain regions [1-5]. This claims that there would be a relation in the phase dynamics of the oscillations in the non-identical local neural populations. In previous studies, the synchronization degree was estimated with a method presented [2]. In this approach, the Tass synchronization index is described by the average dynamics of the phase difference among various spatial oscillators over a time window assuming this analytic dynamic is stationary over the given time interval. The Hilbert transform is used to obtain complex dynamics. The Hilbert transform is a fundamental mathematical operator in many different areas because there is a close relation to causality [6]. It states that the real- and imaginary parts of a causal signal are related by the Hilbert transform which constructs an analytic signal in complex space. Gabor has proposed the Hilbert transform who has proved that all information about the analytic signals compact in the amplitude of the signal [6]. Moreover, the phase of the signals can be calculated from the amplitude and its conjugation (imaginary part) from Hilbert Transform. This means that Hilbert Transform causes to two-dimensional embedding of the limit cycle which is called strange attractor. The analytic signal z_t can be represented in Equation (1):

$$z_t = v_t + iv_t{}' = A_t e^{j\phi(t)}$$
$$v_t{}' = \frac{1}{\pi} p.v. \int_{-\infty}^{\infty} \frac{z(\tau)}{t-\tau} d\tau \quad (1)$$

in one channel, j where $v(t)$ and $v'(t)$ are the real and imaginary parts of the analytic signal. $p.v$ denotes the Cauchy principal value of the singular integral. After Hilbert transform is applied to each channel separately, we obtain an analytic signal $z_j(t)$.Analytic amplitude,$A_j(t)$ was obtained by $A_j(t) = \sqrt{v_j^2(t) + v_j'(t)^2}$. The analytic phase of each channel, $\varphi_j(t)$ for the $j = 1 \ldots 18$ electrodes were given by the arctangent of the ratio of the imaginary part of the real part as shown in Equation (2). The analytic phase is discontinuous and jumps from $-\frac{\pi}{2}$ to $\frac{\pi}{2}$.

$$\varphi_j(t) = \tan^{-1} \frac{v_j'(t)}{v_j(t)} \quad (2)$$

The analytic amplitude for each channel $A_j(t)$ is the norm of each sampled point as shown in Equation (3).

$$z_j(t) = v_j(t) + iv_j'(t) \quad (3)$$

The degree of synchrony was based on Hilbert Transform proposed by a method. Tass applied the method to each channel independently [7]. Tass index is calculated which is based on distributions of Shannon entropy values of phase differences of a sliding window during the time interval assumed stationary for each electrode pair.

We obtained Tass Index by implementing $\Delta\varphi(t)_{i,j} = \left|\varphi_i(t) - \varphi_j(t)\right|$ spatial phase difference signals between i and j channels over predefined window length, $T\ (msec)$. The index was generalized to channel pairs by calculating the distribution (histogram) of complex differences $\Delta\varphi(t)$ after subtracting the means for each coupled electrode pair within sliding window length in T msec. The window length was estimated at two times the frequency at the peak of the Power Spectral Density-PSD_T of the spatial averaged EEG channels after band-pass FIR filter is applied. The window length was applied at the sampling period $f_s = 125\ Hz$ over total 350-sec recording time. In Tass synchronization index, Shannon entropy can be defined based on (normalized histograms) p_k of phase difference distributions, $\Delta\varphi(t)_{i,j}$ given in time window as shown in Equation (4).

$$e(t) = -\sum_{k=1}^{N} p_k \ln\ p_k \quad (4)$$

where $p_k(t)$ probability was the relative distribution of phase values $\Delta\varphi(t)_{i,j} mod\ 2\pi$ difference signals between i and j electrode within the k. th. bin. The number of bins is (i.e. $N = 100$). This synchronization index changes instantaneously. This index is normalized by $\hat{e}$ thus the index changes between zero and one as shown in Equation (5).

$$q(t) = (\hat{e} - e(t))/\hat{e} \quad (5)$$

where $\hat{e} = \ln N$ as constant and N is the number of bins (e.g. 100 bins of 0.06 radians of resolution between $-\pi$ and $+\pi$ radians). The $q\ (t)$ was zero

for a uniform distribution and one for a delta distribution of phase values [8].

2. GENERAL REQUIREMENTS

We define multichannel EEG signals over a predefined window length of d sampling steps, which lasts $T_w = d * (1/f_s)\ (msec)$. Then, we define $\mathbb{C}^d$ space which defines the sliding window of complex dimension n for each electrode. Throughout this paper, we slide the window over all samples, in $z \in \mathbb{C}^d$ as column vectors in $d \times 1$ matrix form $z = (z_{t-1}, \dots, z_{t-d})^T$, where the symbol T stands for the transpose of the vector. For $z \in \mathbb{C}^d$, the conjugate of z, denoted by $\bar{z}$, is defined by $\bar{z} = (\bar{z}_{t-1}, \dots, \bar{z}_{t-d})^T$. For $z \in \mathbb{C}^d$ and $w = (w_{t-1}, \dots, w_{t-d})^T \in \mathbb{C}^d$, we write the inner product $\langle z, w\rangle := \sum_{t=1}^{d} z_t \bar{w}_t$ and in other words $|z| := \langle z, z\rangle^{1/2} = (|z_{t-1}|^2 + \cdots + |z_{t-d}|^2)^{1/2}$ which is the sum of analytic amplitudes. In another word, $|z| :=< z, z >$ also denotes the dissipative power of the frame after de-meaning. The expectation value of each window at each electrode can then be explained within $a = (a_1, \dots, a_1)^T \in \mathbb{C}^d$, copies of a_1 complex values with $n-$ times. we set $\mathbb{B}^d(a, r) = \{z \in \mathbb{C}^d : |z - a| < r\}$. We transformed d-dimensional $\mathbb{B}^n$ the ball into the unit ball $\mathbb{B}^d(0,1)$ by dividing each de-meaned sample value with $|z|$ and letting $\mathbb{B}^d(0,1) = \{z \in \mathbb{C}^d : |z - a| < 1\}$ which explains normalized complex pseudo-variance.For $z, w \in \mathbb{D}$ acquired sliding vectors from an electrode pair, the pseudo-hyperbolic distance is defined [7] as shown in Equation (6).

$$\rho(z, w) = \left|\frac{z-w}{1-\bar{w}z}\right| \qquad (6)$$

representing simultaneous (or conjunctive) presence presynaptic firing of neural populations z and postsynaptic firing populations w at different regions.

We introduced a new Entropy Synchronization index improved from the Tass Synchronization Index. First, we define two pairs of channels (vectors) over window length for $z, w \in D$ within the unit disk (normalized). Let $z^i = (z_t, z_{t-1}, \dots z_{t*T-1})$ and $z^j = (w_t, w_{t-1}, \dots w_{t+T-1})$, $i \neq j$ complex vectors from i and j electrodes with T representing a sliding time window in msec. Complex spatial differences of each of two vectors (windows) over the scalp can represent synchronization better due to including both phase and amplitude coupling of spatial synchronization scheme simultaneously. The system architecture is shown in Figure 1.

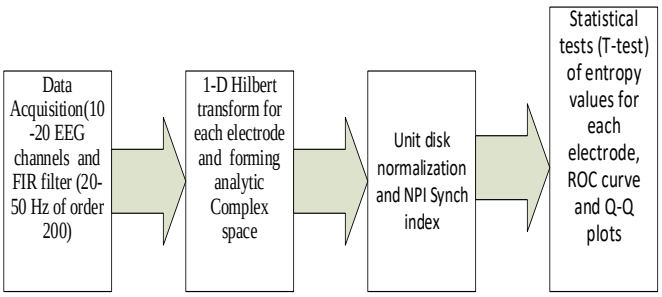

Figure 1 The architecture of the information pipeline

The pseudo-hyperbolic distance acquired from each paired vector represents L distribution from one source electrode, i, to other all possible representing spatial phase difference combinations over a time window. We implement a pseudo-hyperbolic distance function with its denominator is the inner multiplication of conjugate of $\bar{w}$ and z for each electrode pair, respectively. The distance represents both anti-correlation and the analytic difference between two electrodes paired as shown in Figure 2. This is an example of whether 6 electrodes are used. Properties of K_n topology with the $n = 10 - 20$ electrode configuration:

- Each vertex in K_n has degree $n - 1$.
- K_n has $n(n-1)$ directed non-commutative edges explaining both top-down and bottom-up directions on the same edge which is the first approach.
- K_n contains the all directed edges out of graphs on n vertices.

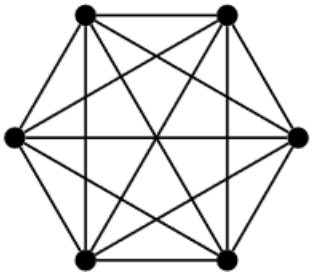

Figure 2 Complete topology of n =6 electrode K_6 connectivity. Each vertex represents an electrode from {Fp1, Fp2, ...} running through a time window of w^j, z^i vectors. Each index has a fan-out connection associated with pseudo-hyperbolic distances to other $L = (n-1)$ electrodes

The inner product of two complex vectors of all electrodes is the complex correlation distribution of whole EEG activity at each time window. Superscripts $\{i, j\}$ pair denotes electrode location numbers such as $\{Fp1, Fp2, \ldots\}$. From one channel indexed i to distances of all other channels excluding itself can give a fan-out degree of $L = (n-1)$ and $n = 18$ with the following equation (7) with an edge of K_{18} connectivity

$$\rho_i(z_t, w_t) = \sum_{k=1}^{L} \left| \frac{z_t^{\{i\}} - w_t^k}{1 - \bar{w}_t^k z_t^{\{i\}}} \right| \quad (7)$$

U denotes the total number of time windows, $t = 1, \ldots U$. Instantaneous pseudo-hyperbolic distance at a given t is normalized as $\overline{\rho^t} = \rho_i(z_t, w_t) / max\{\rho_i(z_t, w_t)\}$ from one channel distance divided by the maximum of all other L distances. In other words, the maximum operator is taken over all fan-out degrees of each electrode at a given time index, t. We finally obtain a distribution of normalized pseudo-hyperbolic distances as probability values over whole all-time windows either overlapped or non-overlapped. We then embedded pseudo-hyperbolic distance distributions into a Shannon entropy function representing probability distributions, $0 < \overline{\rho^t} < 1$ of one source to other all destinations derived from spatial phase distribution of histograms. Stochasticity is an inevitable characteristic of brain dynamics. We investigate the entropy of each electrode, i defined as ranging

$$e^{\{i\}}(t) = -\overline{\rho^t} \ln \overline{\rho^t} \quad (8)$$

through all U time windows as shown in Equation (8).

We then define the synchronization index which denotes the flexibility of pseudo-hyperbolic distance over all time windows for each electrode. NPI syn index for the i .th electrode can be defined in Equation (9) as

$$\overline{\Delta e_{Syn}^i} = \frac{\underbrace{max}_{U}(e^i) - \underbrace{min}_{U}(e^i)}{\underbrace{max}_{U}(e^i)} \quad (9)$$

The novel NPI syn index explains entropy change flexibility of fan-out degree in a given electrode.

3. THE RESEARCH FINDINGS AND DISCUSSION

In this study, 10-20 channel EEG data signals are filtered within a frequency band (20-50) Hz that includes beta-gamma frequency ranges. Using the phase and amplitude synchronization entropy paradigm, it was found that there was a significant difference between the resistive and non-resistive treatment groups in the beta-gamma band for the T3, T4, and Pz electrodes. Beta-gamma band represents cognitive deficits in OCD disorders [8].

This study showed that a decrease in beta-gamma power and phase synchrony with the relation of cognition in resistive patients with higher entropies. 14 patients with non-response to treatment and 20 patients with response to treatment in age from 20-55 years. They were recruited from Uskudar University NPI Hospital, Uskudar, Turkiye. The patients were diagnosed according to DSM-IV and World Health Organization ICD-10 for OCD. All patients were receiving medication at the time of recording and one group responded to treatment and the other group did not respond to medication.

For EEG paradigms, 10-20 electrode montage was recorded with removing eye-blinks artifacts through visual inspections. Moreover, EEG signals are analog filtered with an analog bandpass filter at 0.5-70 Hz with a 12-bit

resolution. A Notch filter is used for rejecting 50 Hz power line frequency. The sampling frequency $f_s$is set to 125 Hz. The sampling frequency is at least twice as high as the signal highest frequency ($f_s \approx 50$) which complies with the Nyquist theorem. Each subject was acquired for a 350 second (43750 data points) trial period corresponding to eyes-closed conditions. 19-channel EEG signals are demeaned to remove channel bias. A temporal band-pass FIR filter with an order of 200 was applied to get beta-gamma activity (20-50 Hz). After digital filtering, 10-20 channel EEG data for each subject are normalized to unit standard deviation(SD).

We found a significant condition effect for Fp2 ($p < 0.001$). The confidence level is 0.001. T3 and T5 are the electrodes that show the most significant differences for Δe_{NPI} over 12-50 Hz range.

We applied two different types of classification approaches for comparison. Logistic Regression and Support Vector Machine (SVM) as shown in figure 3 and figure 4 respectively. The estimated coefficients perfectly separate failures from successes for the selected channels with ($p<0.001$) as shown in Table 1.

Table 1 The p-values of two groups, response to treatment and non response to treatment groups

Fp1	0.013826
Fp2	5.101e-05
F3	0.10296
F4	3.139e-05
C3	3.661-e08
C4	3.893e-08
P3	0.0010078
P4	0.11867
01	1.72e-09
02	8.46e-10
F7	2.35e-08
F8	0.0030742
T3	4.91e-09
T4	1.18e-07
T5	8.91e-09
T6	1.092e-05
Fz	0.03221
Cz	2.9179e-08
Pz	1.3301e-08

For the fitted linear combination XB (entropic rate threshold) of the predictors, the sample proportions P of Y=36 from two groups in the data satisfy: XB <-0.253052: P=0 (OCD Response to treatment), XB>-0.253052: P=1 (OCD Nonresponse to treatment).

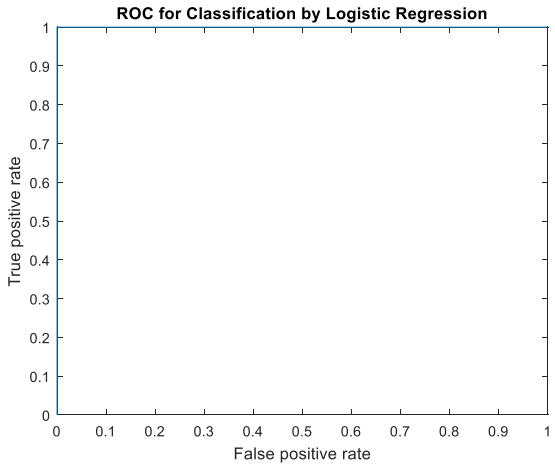

Figure 3 ROC Curve of Logistic Regression Classification for two groups (treatment response v.s. non-treatment response) using NPI Synch Index

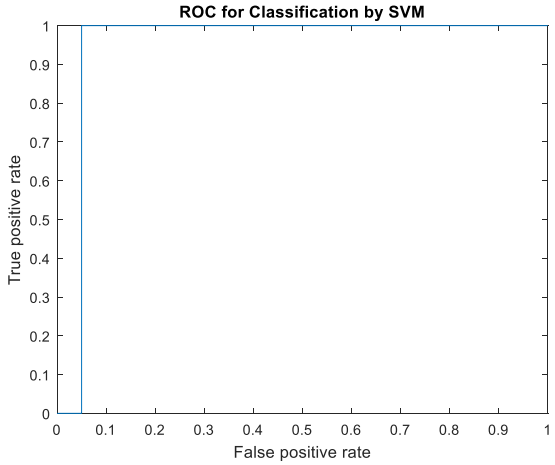

Figure 4 Support Vector Machine Classification for two groups (treatment response v.s. non-treatment response) using NPI Synch Index

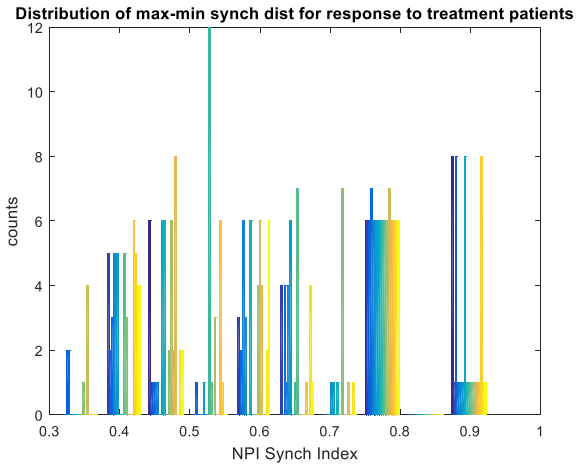

Figure 5 NPI Synchronization Index values distribution of beta-gamma band of EEG signals for a treatment response OCD patient at the full number of time windows. The vertical axis denotes the number of time windows

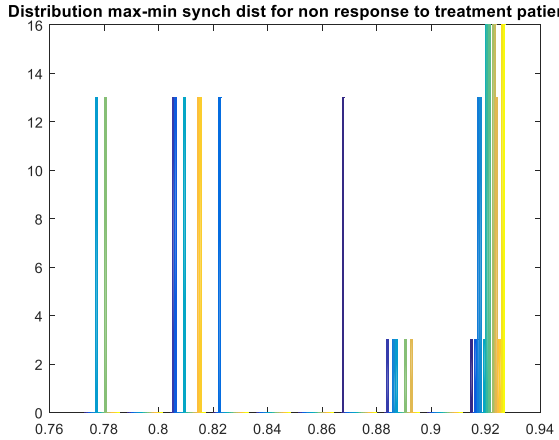

Figure 6 NPI Synchronization Index values distribution of beta-gamma band of EEG signals for a non-response to treatment resistance OCD patient at a full number of time windows. The vertical axis denotes the number of time windows

We concluded that NPI Synch Index distribution is a range of wide interval for response to treatment patients $(0.32 \leq NPI \leq 0.9)$ as shown in Figure 5 whereas this distribution changes over the very small interval $(0.78 \leq NPI \leq 0.93)$ for non-response to treatment patients as shown in Figure 6 during beta-gamma phase transitions. Q-Q statistical analysis of results demonstrated significance level between two groups (very significant deviation from linearized as one

group). Results display quantile-quantile plots of the one channel sample data for all cases versus the quantiles of the sample data of another channel over whole cases. If the samples come from the same distribution, then the plot appears linear. Q-Q plots as shown in Figure 7 and Figure 8 reveal that non-response to treatment patients do not change the standard normal quantiles over quantile of synchronization values, respectively. The patients' values are distinct depending on the patient clinical evaluations.

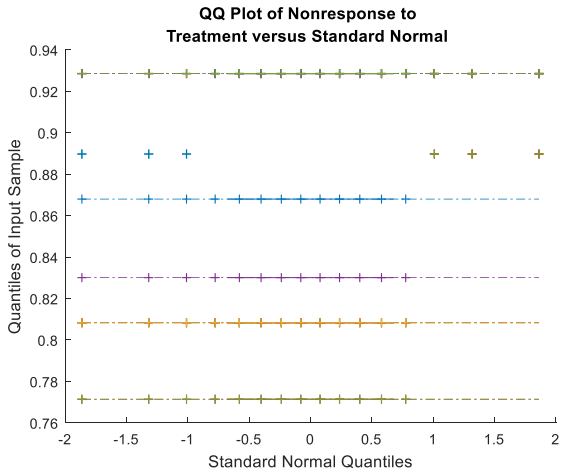

Figure 7 QQ Plots of treatment-resistant group

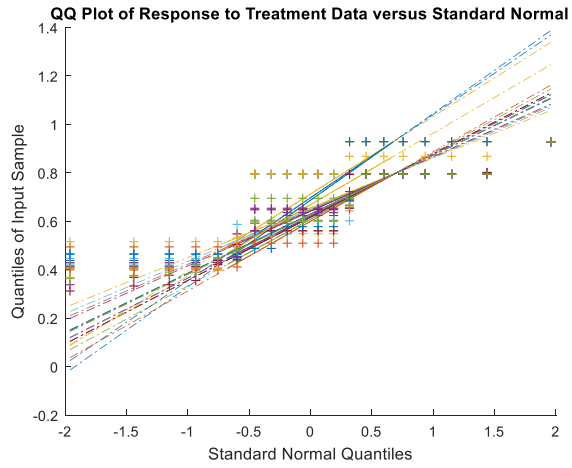

Figure 8 QQ Plots of response to treatment group

Acknowledgments

We would like to thank Prof. Dr. Nevzat Tarhan, for comments on manuscript. This work is supported by Üsküdar University NPI hospital under the Neuroimaging Research Group. That's why the developed biomarker was called the NPI Syn index.

Funding

The author (s) has no received any financial support for the research, authorship or publication of this study.

The Declaration of Conflict of Interest/ Common Interest

No conflict of interest or common interest has been declared by the authors.

Authors' Contribution

The author contributed 100 % to the study.

The Declaration of Ethics Committee Approval

This study does not require ethics committee permission or any special permission.

The Declaration of Research and Publication Ethics

The authors of the paper declare that they comply with the scientific, ethical and quotation rules of SAUJS in all processes of the paper and that they do not make any falsification on the data collected. In addition, they declare that Sakarya University Journal of Science and its editorial board have no responsibility for any ethical violations that may be encountered, and that this study has not been evaluated in any academic publication environment other than Sakarya University Journal of Science.

REFERENCES

[1] Freeman, Walter J.. "Origin, structure, and role of background EEG activity. Part 1. Analytic amplitude," Clinical Neurophysiology 115 (2004): 2077-2088.

[2] L Tass, P., Rosenblum, M. G., Weule, J., Kurths, J., Pikovsky, A., Volkmann, J., …

Freund, H.-J. (1998). "Detection of n:m Phase Locking from Noisy Data: Application to Magnetoencephalography," Physical Review Letters, 81(15), 3291–3294.

[3] Freeman, W. J., & Rogers, L. J. (2002). "Fine temporal resolution of the analytic phase reveals episodic synchronization by state transitions in gamma EEGs. Journal of Neurophysiology," 87(2).

[4] Kamaradova, D., Hajda, M., Prasko, J., Taborsky, J., Grambal, A., Latalova, K., Hlustik, P. (2016). "Cognitive deficits in patients with obsessive-compulsive disorder -electroencephalography correlates. Neuropsychiatric Disease and Treatment," 12,1119–25.

[5] Chen, Shaolin and David Kalaj. "Lipschitz continuity of holomorphic mappings with respect to Bergman metric," arXiv: Complex Variables (2017): n. pag.

[6] Koppleman W and Pincus JD, (1959) "Spectral representations for finite Hilbert transform," Math Z. vol. 71, pp. 399-407.

[7] Tass P, Kurths J, Rosenblum M, Weule J, Pikovsky A, Volkmann J, Schnitzler H, Freund H. In: Uhl C, editor. (1999), "Complex phase synchronization in neurophysiological data. Analysis of neurophysiological brain functioning," Berlin: Springer. p. 252–73.

[8] Freeman, Walter J.. "A pseudo-equilibrium thermodynamic model of information processing in nonlinear brain Dynamics," Neural networks : the official journal of the International Neural Network Society 21 2-3 (2008): 257-65.